International Journal on Advanced Science Engineering Information Technology

Vol.11 (2021) No. 5
ISSN: 2088-5334

Effect of Land Cover on Tsunami Overland Flow Propagation: A Case Study of Painan, West Sumatra, Indonesia

Mohammad Bagus Adityawan[a], Puspita Rahmasari[b], Asrini Chrysanti[c,*], Mohammad Farid[c,d], Bagus Pramono Yakti[d], Muhammad Rizki Purnama[e]

[a]*Department of Water Resources Management and Engineering, Institut Teknologi Bandung, Jatinangor, West Java, 45363, Indonesia*
[b]*Graduate Student of Structural Engineering, Institut Teknologi Bandung, Bandung, West Java, 40132, Indonesia*
[c]*Water Resources Engineering Research Group, Institut Teknologi Bandung, West Java, 40132, Indonesia*
[d]*Center for Coastal and Marine Development Institut Teknologi Bandung, West Java, 40132, Indonesia*
[e]*Graduate Student of Water Resources Management, Institut Teknologi Bandung, West Java, 40132, Indonesia*
Corresponding author: [*]asrini@ftsl.itb.ac.id

***Abstract*—Tsunami overland flow may cause severe destruction to the affected coastal area. Several tsunamis had hit Indonesia. Studies have shown that there is a high probability of a massive earthquake in the Mentawai fault, Sumatra, Indonesia. A massive earthquake with a magnitude of over 8 Mw might occur in the next 50 years. The nearshore tsunami propagation and inundation in Painan City, West Sumatra, Indonesia, is assessed using HEC-RAS. Various land cover types are simulated to investigate their effects on the tsunami overland flow. The model showed satisfactory results. The model can show the known behaviors of tsunami propagation in urban areas and in rivers. It was found that there is a significant effect of land cover types on the inundation at the coast. Inundation depth increases with roughness along the coast. On the other hand, high roughness decreases the inundated area. Furthermore, the land cover has a significant effect on the velocity. The velocity is much lower in higher Manning's value. Simulation with a high surface roughness shows a significant reduction in both inundation area and velocity. The high roughness causes a blockage effect for tsunami propagation. Thus, the Tsunami cannot penetrate further inland. The information can be used for land use control suggestions. These provide significant information for future mitigation plans, e.g., placement of evacuation buildings and evacuation routes.**

***Keywords*— Tsunami; inundation; overland flow; land cover; roughness.**

Manuscript received 17 Jan. 2021; revised 16 Feb. 2021; accepted 15 May 2021. Date of publication 31 Oct. 2021.

I. INTRODUCTION

Indonesia lies between two geological plates, the Australian plate, and the Eurasian plate. Thus, Indonesia is vulnerable to earthquake and tsunami disasters. Tsunami is a gigantic wave caused by plate movements underwater, i.e., underwater earthquakes, underwater volcanic activity, underwater mudslide, or meteor-laced land. There have been many tsunami events that occurred in Indonesia throughout the decades. The two biggest events are the Krakatau eruption in 1883 and The Great Indian Ocean Tsunami in 2004. The Tsunami of Krakatau in 1883 has killed about 36,000 people. The Great Indian Ocean Tsunami in 2004 caused fatalities of 128,645 persons, with over 37,063 persons missing and 532,898 persons displaced [1]. The ruptured 1,200–1,300 km segment of megathrust extending from offshore northern Sumatra to the Andaman Islands generated the Tsunami [2]. The Tsunami devastated hundreds of kilometers of the northwest Sumatra coast, with the maximum tsunami wave were greater than 12 meters [3].

After the 2004 Indian Ocean Tsunami, studies on earthquakes and Tsunami in Indonesia mostly focused on Sumatra Island. Sumatra island is surrounded by the converging of the Australian and Eurasian plates, called the Sunda fault. In the past decades, ruptured occurred sequentially in several sections of the Sunda fault. The largest rupture occurred on March 28, 2005, Nias (8.6 Mw), rupturing the Sunda fault following the Great Indian Ocean Tsunami in 2004 (9.1 Mw). The event has raised great concern about the unbroken Mentawai fault. The study estimated that the Great Indian Ocean Earthquake in 2004 increased the stress on the megathrust to the south, one of which is under the Mentawai islands [4].

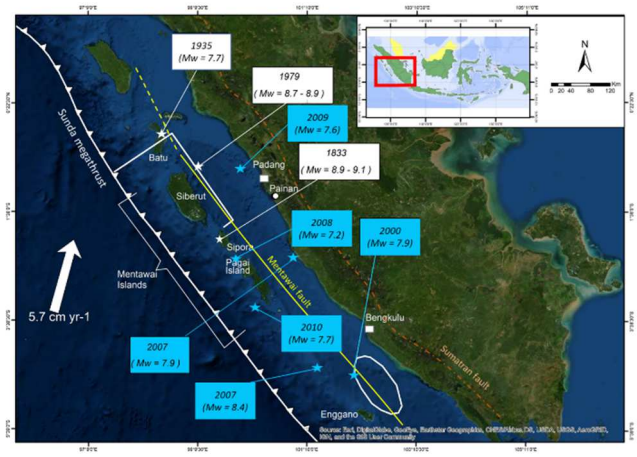

Fig. 1 West Sumatra subduction zone and historical earthquake.

The Sunda fault lies throughout Mentawai Island (Fig.1). The Sunda megathrust is marked with a solid white line with the one-sided arrow indicating the shearing motion. The Mentawai fault (yellow line) and the Sumatran fault (orange line) are also shown. The epicenters of the previous rupture events are marked with a star. The rupture events adjacent to the Mentawai islands are marked with the year of the event and the earthquake magnitude. Blue stars indicate the recent large earthquakes. The relative shearing plate motion relative to the Sunda fault is marked with a one-sided arrow along with the plate. The Mentawai fault is divided into two segments. The Siberut segment and the Sipora-Pagai segment. Before 2004, the 700-kilometer-long unbroken Mentawai segment ruptured in the past decades. Two great earthquakes occurred in 1797 at Siberut (8.7 Mw) and in 1833 at Sipora-Pagai (8.4) Mw [5]. Since 2004, the segment ruptured in a series of events. An 8.4 Mw and a 7.9 Mw occurred on September 12, 2007. These were followed by a 7.7 Mw event on October 25, 2010, in the south of the Mentawai fault within the ruptured area of the 1833 event. The 2007 and 2010 events show the change in rupture behavior in the southern of the Mentawai fault. Several smaller magnitudes of earthquake occurred, rupturing the smaller portion of the segment instead of the whole segment in one large earthquake [6]. Following the 2007 events, a 7.2 Mw earthquake occurred at Pagai island in 2008, and a 7.6 Mw in 2009 occurred on the northern edge of the Mentawai fault. Consequently, as the 2007 and 2010 events only ruptured the southern section of the Mentawai fault, the potential for a large earthquake to occur on the northern section of the Mentawai fault within the area of the 1979 rupture remains high.

Geodetic and paleo geodetic measurements have revealed that the displacement within the Mentawai area was not sufficient. The slip deficit accumulated in the area has exceeded the slip during 1797 and slowly reaching the slip during the 1833 earthquake. This indicates that the unbroken Mentawai fault may already be advanced in the seismic supercycle. Both segments have a return period of 200 to 250 years of the earthquake [7]. The sequence failure is persistent in the Mentawai segment. Most of the ruptures terminate between the south of Siberut and the strait of the Pagai Islands. Although the rupture cascades on the Mentawai segment occur approximately every 200 years, the largest earthquakes occur separated by 40 years (1797 to 1833) [8]. Based on this speculation, the large earthquake triggering a tsunami of over 8 Mw might be possible in the near decades [9]. Therefore, West Sumatra has a high probability of a massive rupture earthquake from the Mentawai fault.

The Sunda megathrust and the back thrust of the Mentawai fault (Fig. 1) have a high possibility to generate a tsunami wave. The back thrust possessed a direct threat to the western coast of Sumatra [10]. The Tsunami generated by the back thrust may arrive faster than that by the megathrust. It may also cause severe damages to the area. The Mentawai fault is located very close to the West Sumatra coastline. A tsunami can be a significant threat to nearby cities, such as Padang, Painan, and Pariaman. The cities along the coastline of West Sumatra are highly populated areas and vulnerable to Tsunami. Many researchers assess tsunami in cities i.e., Padang, Bengkulu, Pariaman, and Painan [11]–[13]. The studies stated that the maximum tsunami wave height reaches up to 10 meters in Padang and Painan. The tsunami arrival time on the west coast of West Sumatra from the Mentawai fault rupture is less than an hour. It takes about 30 minutes to reach the west coast of West Sumatra for an 8.9 Mw scenario. Therefore, mitigation is crucial to minimize the impact of a tsunami hazard in the area. Unfortunately, a Tsunami's inundation process is still difficult to be modelled due to complex interactions between the wave propagation and the overland flow [14]. The various assessment has been performed to have a better understanding of tsunami process. The study can be conducted based on analytical, laboratory, and numerical experiments. The last is being the most widely used.

Various researchers have performed Tsunami simulations. The tsunami model may provide an accurate estimation of tsunami propagation and inundation. Various software has been developed. MOST (Method of Splitting Tsunami) was used to model the tsunami generation and the tsunami inundation in West Sumatra [15]. MIKE21 also performed well to simulate the inundation based on roughness in Indonesia [16]. DELFT3D has been used to simulate tsunami inundation and the transport of sediment [3]. COMCOT (Cornell Multi-grid Coupled Tsunami Model) also has been tested with several experiments and shows an ability to simulate tsunami inundation, sediment transport, and morphological changes. A case study of tsunami assessment in Painan City had been conducted using COMCOT and showed appropriate results [17]. These models can simulate the tsunami wave from the source (fault) to the coastal area. However, they may not be flexible and user-friendly, especially for a nearshore tsunami simulation. The nearshore tsunami propagation and inundation are highly important in mitigation.

HEC-RAS is generally used to simulate flood waves in rivers and dams. The model was developed based on the Shallow Water Equation (SWE) [18]. SWE is commonly used for tsunami simulation, especially in coastal areas [19]. HEC-RAS has been widely applied to simulate dam-break flow, which is similar to a nearshore tsunami [20]. The software has a friendly user interface. It is also integrated with GIS. HEC-RAS can simulate the run-up of long-wave over a frictionless planar slope. The wetting and drying performance is considered satisfactory [21].

Tsunami overland flow propagation is highly affected by the surface condition. This condition is often represented as roughness. Deciding the right roughness value is crucial to obtain an accurate result [22]. Furthermore, there are challenges to simulate tsunami propagation in urban areas. Paths and flow patterns change due to buildings and road alignment. The influence of roughness on water flows was discussed in previous studies [23]–[25]. Other studies stated that buildings in urban areas could act as barriers or protectors. Barriers can influence inundation patterns [26]. Jakeman *et al.* [27] stated that buildings are useful as energy absorbers. They also reduce the volume of water on the beach. However, the flow velocity increases between buildings or roads. These are also consistent with previous studies [25,28]. They stated that tsunami propagation in rivers and roads has a greater height due to narrowing and mild slope.

Dao and Tkalich [29] studied the roughness effect on tsunami propagation. They showed that roughness has a significant effect on the tsunami height. Vegetation and buildings such as bridge pillars can act as a barrier. Although building might act as a barrier, additional coastal protection effectively reduces the tsunami impact [30]. Another study also found that the tsunami effect was significantly reduced due to mangroves' presence [31]–[35]. This also shows that building and vegetation has a significant effect on wave propagation and inundation patterns. Another study has also found that wave velocity inside the buildings is much slower than in open areas [28].

Roughness is very important in shallow water. It has a significant influence on inundation patterns. Therefore, it is very important to consider this phenomenon in tsunami modelling. The structure can be represented by its height or as a very rough surface. Most models use surface roughness in their approach [22], [23]. Surface roughness is usually estimated using Manning's values. Various of Manning's values have been proposed. A value of 0.063 was proposed for low-density urban areas [36]. On the other hand, another study found that Manning's value of 0.04 must be applied under the same land cover condition [37]. The results of several studies show different manning's values.

This study investigates the effect of various surface conditions on the tsunami overland flow in Painan City. The nearshore tsunami propagation in Painan City is simulated using HEC-RAS. The model is used to simulate the near coast tsunami. The rupture scenario and the incoming wave were assessed from the previous study using the potential rupture in the unbroken of the Mentawai fault [21]. Three scenarios of manning's value were selected, and the effect of manning's value on tsunami inundation were compared. The result of the study is expected to provide a better understanding of the effect of roughness on tsunami inundation.

II. Material and Method

A. Study Area

This study was carried out in Painan City, West Sumatra, Indonesia. The city is located 78,4 km south of Padang (Fig. 2). Painan City is selected because it is very close to the tsunami source in the Mentawai Fault. A large earthquake triggering a tsunami on a scale similar to the Indian Ocean 2004 might be possible in the near decades.

Painan City has a large population of 420,000 people. The city is located along the west coast of Sumatra. In the past decade, the evidence of cascade rupture sequence in the Mentawai fault has attracted many researchers to investigate the fault characteristics and future rupture possibilities. The past tsunami event in 2007 is believed to only released partial energy, and a significant section of the Mentawai fault may rupture soon. The most recent event in 2010, a rare type of earthquake occurred in the Mentawai fault and generated a tsunami much larger than expected based on the seismic magnitude [38]. The shallow rupture generated a tsunami of approximately 6 meters. The uncertainties of these rupture characteristics raise concerns for the upcoming earthquake.

Fig. 2 Location of study

The heaviest casualties occurred in Sabeugukgung Village, which is located at the back of the bay. The village is surrounded between the ocean and the river on the other side. The stream prevents the villagers from evacuating to the higher ground. As a result, the majority of the villagers were killed by the Tsunami [38]. Painan City's geographical conditions are similar to that of Sabeugukgung Village. The city is located in a bay and surrounded by hills in the upstream area. A river also runs through Painan City. In addition, Painan City has a much higher population than Sebeugukgung Village. Therefore, the study of tsunami propagation and inundation may provide significant information for mitigation in this area.

B. Numerical Model

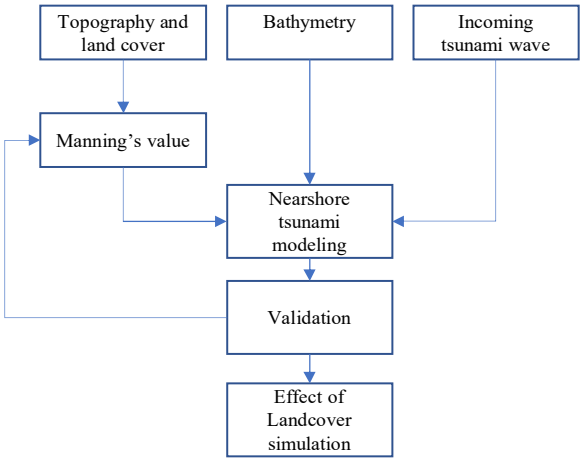

Fig. 3 Research Flow Chart

The flowchart of this study is shown in Fig. 3. The incoming tsunami wave simulates nearshore tsunami propagation and inundation over the coast of Painan City. Simulation is conducted using HEC-RAS v. 5.0.7. The HEC-RAS solves the full 2D Shallow Water Equations (SWE):

Continuity Equation:

$$\frac{\partial h}{\partial t} + \frac{\partial (hu)}{\partial x} + \frac{\partial (hv)}{\partial y} = 0 \quad (1)$$

$$\frac{\partial h}{\partial t} + \frac{\partial (hu)}{\partial x} + \frac{\partial (hv)}{\partial y} = 0$$

Momentum Equation:

$$\frac{\partial hu}{\partial t} + \frac{\partial hu^2}{\partial x} + \frac{\partial huv}{\partial y} = -gh\frac{\partial (h+z)}{\partial x} - \frac{n^2 g\,|\sqrt{u^2+v^2}|}{h^{1/3}}\,u \quad (2)$$

$$\frac{\partial hv}{\partial t} + \frac{\partial huv}{\partial x} + \frac{\partial hv^2}{\partial y} = -gh\frac{\partial (h+z)}{\partial y} - \frac{n^2 g\,|\sqrt{u^2+v^2}|}{h^{1/3}}\,v \quad (3)$$

where h is water depth (m), z is the bed elevation (m), u and v are the velocities in the Cartesian directions (m/s), n is the Manning coefficient, g is gravity (m/s2). The value of n highly depends on the land cover condition.

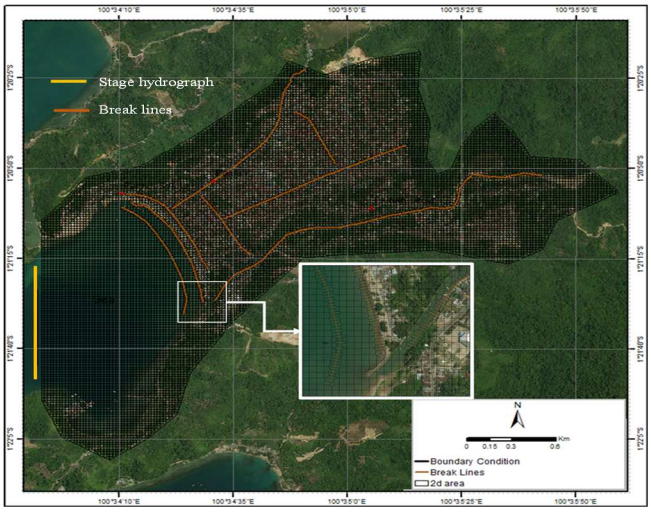

Fig. 4 Model setup

This study simulates the tsunami wave propagation from the mouth of Painan Bay and its overland flow on Painan City. The far-field Tsunami from the source is not simulated. As presented in the previous study, the incoming tsunami wave at Painan Bay was generated from an 8.92 Mw at the Mentawai Fault [21]. The model domain is shown in Fig. 4. The incoming tsunami wave (Fig. 5) was applied as a stage hydrograph at the boundary condition. The incoming wave's initial time is the initial earthquake time.

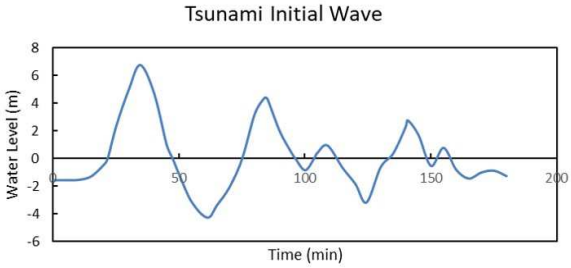

Fig. 5 Stage hydrograph boundary condition

The model domain is divided into grids of 20 m x 20 m. HEC-RAS model employs the linear curve grids as break lines with smaller element sizes. Break lines are used to refine the computational mesh and force the cell faces to align along a specified line. Such break lines may accommodate the challenges in the simulation of tsunami propagation in urban areas. The break lines were added in the domain for roads and a river with 10 m x 10 m grids.

The time step interval was calculated based on the Courant value (0.5–0.8) to ensure the model stability. The water surface tolerance was set to 0.003 m. The nearshore tsunami propagation was simulated for 3 hours. The model setup parameters are given in Table 1.

The bathymetry and topography data were obtained from the Geospatial Information Agency of Indonesia. The bathymetry and topography data have a resolution of 8,1 m x 8,1 m. The surface roughness conditions of Painan City are categorized based on the land cover [39].

C. Scenarios

The land cover roughness is considered to significantly affect the inundation depth, velocity, and arrival time of the Tsunami. The model is simulated based on the categorized land use in the existing conditions Fig. 6. The results are validated with those from the previous study [21]. The effect of surface conditions is further studied using three scenarios. The surface condition for the entire land domain in each scenario is uniform. Manning's value of shallow water and river remains constant for all scenarios (0.025). The scenarios are:

- SC1: Road/open area (Manning's value 0.015)
- SC2: Forest area/mid-density urban area (Manning's value of 0.03)
- SC3: High-density urban area (Manning's value 0.09)

Classification of low, mid, and high-density urban areas is calculated as the building area per hectare. The low density is less than 60%. Mid density was between 60%-80%. High-density was higher than 80%.

TABLE I
MODEL SETUP PARAMETERS

Parameter	Value
Grid resolution (meter)	20 x 20 (open area) 10 x 10 (break lines)
Governing equations	SWE
Time step	Adjust time step based on courant number (0.5 – 0.8)
Water surface tolerance (meter)	0.003
Simulation duration (minutes)	180

Fig. 6 Landcover of Painan City

III. Results and Discussion

A. Model Validation

The initial surface roughness value is estimated based on land use in Figure-6. The selection of Manning's values for different surface conditions can be found in the works of literature [22], [23], [36], [37]. However, the topography data of Indonesia contains the building height above the surface. Therefore, buildings were modelled as both elevation and Manning coefficient. Since the topographical data already includes the elevation of existing buildings, the obtained Manning's value was relatively lower than that from previous studies. At present, Painan City is mostly a mid-density urban area. The value of 0,03 is used for areas with buildings and trees. Manning's value of 0.015 is applied for road and open areas. The shallow water area used Manning's value of 0.025, including for the river.

The simulation results using these values showed a good comparison to those from the previous study [17], as given in Table 2. The simulated maximum depth is shown in Fig. 7. Section A-A is given and shown in Fig. 8. It is also noted that the model can simulate the known phenomenon of tsunami overland flow on urban areas, such as the effect of buildings and roads.

Painan City is severely affected by the Tsunami, with a maximum inundation depth of 6.37 m in the city area (Fig.8). The Tsunami penetrates 1875 m inland; it submerges most of the Painan City. The average depth of the inundation in the city ranges from 2 to 4 m. The averaged inundation depth at the coastline is higher with 8 to 11 m. The wave arrives on the coast approximately 17 minutes after the rupture (Fig. 9). The wave then propagates up to 1.8 km inland within 25 minutes. It is also found that the Tsunami arrives faster in the river. This phenomenon was also reported in the previous study [40], [41].

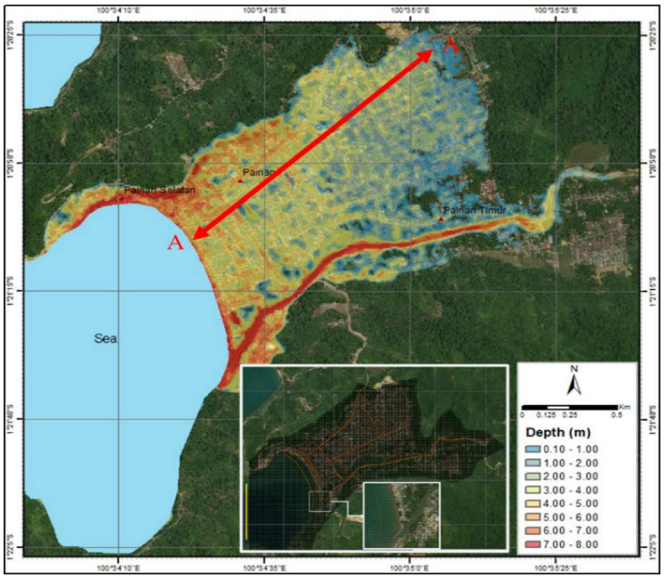

Fig. 7 Maximum Inundation Depth

TABLE II
Model Validation

Parameter	HEC-RAS	COMCOT [21]
Propagation distance	1,875 m	1,884 m
Maximum inundation depth	6.37 m in the city area, 8.3 m in the coastal area	6.8 m in the city area, 7 m in the coastal area
Average inundation depth	Average depth of 2 – 4 m	Average depth of 3 – 4 m
First wave peak arrival time	35 minutes	37 minutes
Velocity	9 m/s in coastal area and 2 – 5 m/s in city area	Average of 2 m/s, reach up to 5 m/s

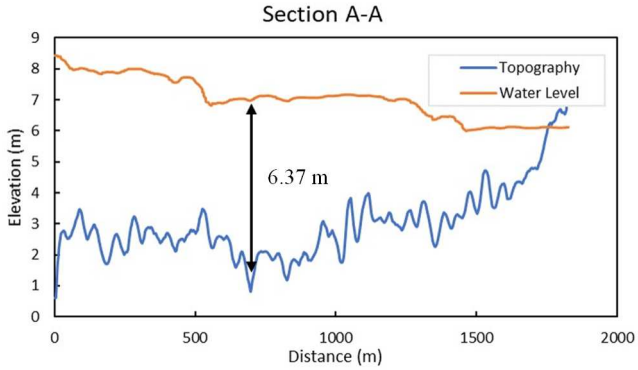

Fig. 8 Water level at section A-A

Velocity distribution varies in the coastal area and in the city area. The maximum velocity reaches up to 9 m/s in the coastal area. The city area's average velocity varied from 2 m/s up to 5 m/s (Fig. 10). The buildings and roads increase the flow velocity in some areas. The spatial distribution of velocity creates line around the building and roads area. It shows similar behavior to that in the river. The buildings' grid layout creates a narrow area and causes the flow to behave similarly to the river.

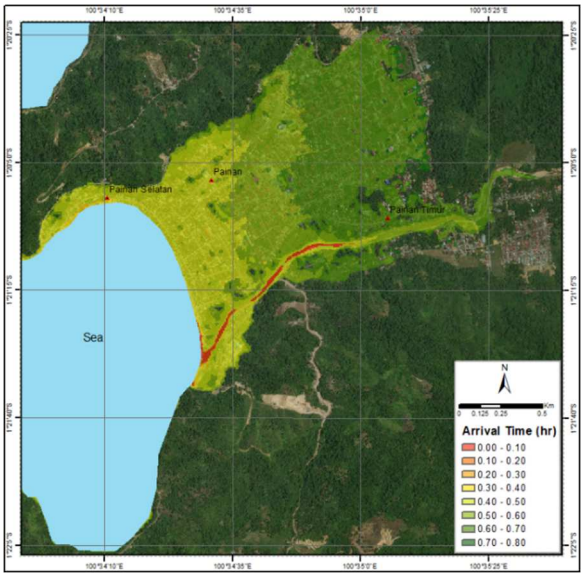

Fig. 9 Arrival time

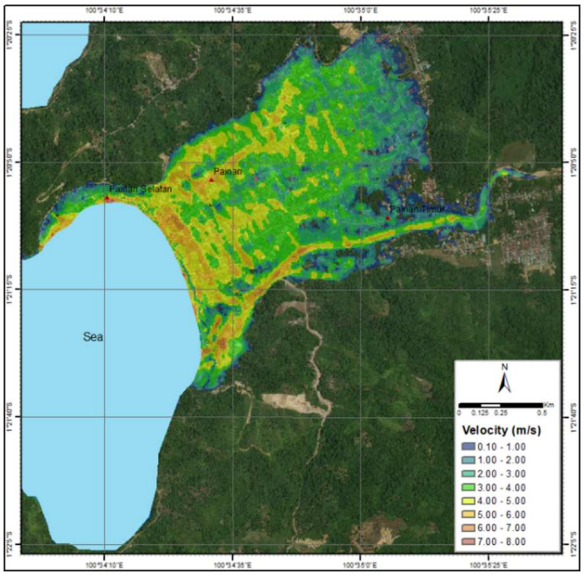

Fig. 10 Maximum velocity

B. *Effect of Landcover*

Three different surface conditions were simulated, as explained in the previous section. The simulation results show that the inundation changes significantly. SC 1 (n=0.015) shows that the Tsunami propagates and inundates a larger area than those of other scenarios (Fig. 11(a)). Open area allows water to propagate easily. In the model, the topography data contains buildings' elevation, as previously explained. Although the Manning's value is assigned evenly distributed in the inland area, the building effect is still visible and can be observed. Less area was inundated in SC2 (n=0.03), as shown in Fig. 11(b). In this scenario, the surface condition is considered as mid-density urban/trees. Nevertheless, the inundation depth is, in general, similar to that of SC1. On the other hand, the SC3 scenario represents a more drastic difference than other scenarios (Fig. 11(c)).

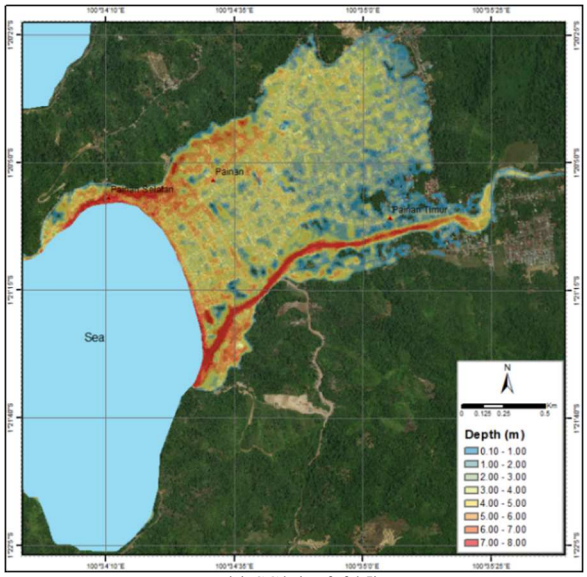

(a) SC1 (n=0.015)

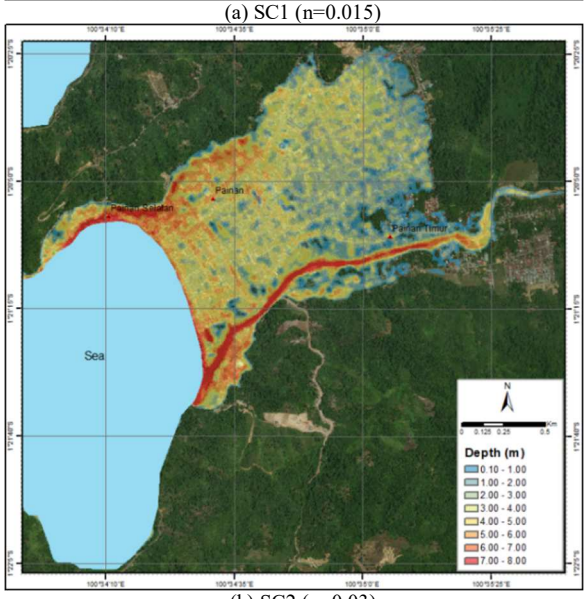

(b) SC2 (n=0.03)

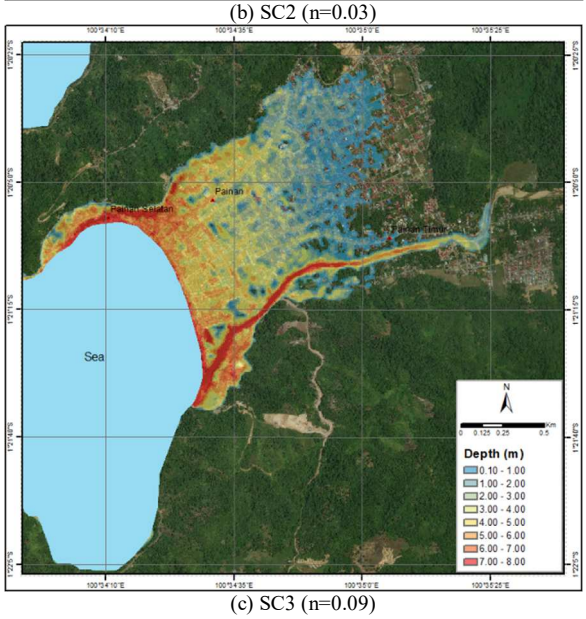

(c) SC3 (n=0.09)

Fig. 11 Maximum inundation depth SC1, SC2, and SC3

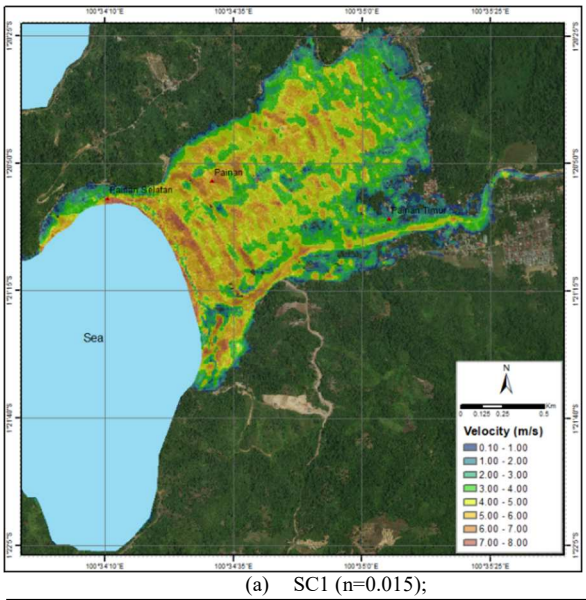

(a) SC1 (n=0.015);

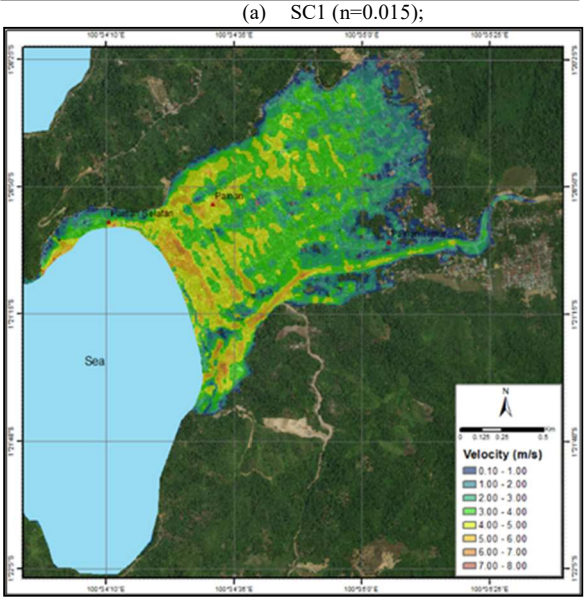

(b) SC2 (n=0.03);

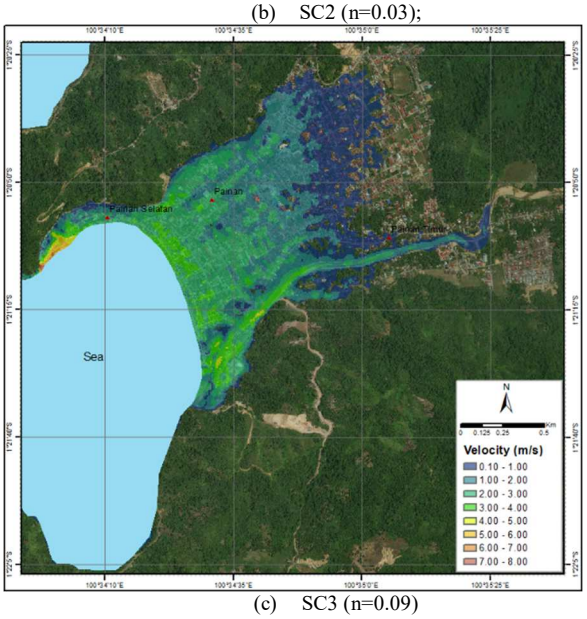

(c) SC3 (n=0.09)

Fig. 12 Maximum velocity SC1, SC2, and SC3

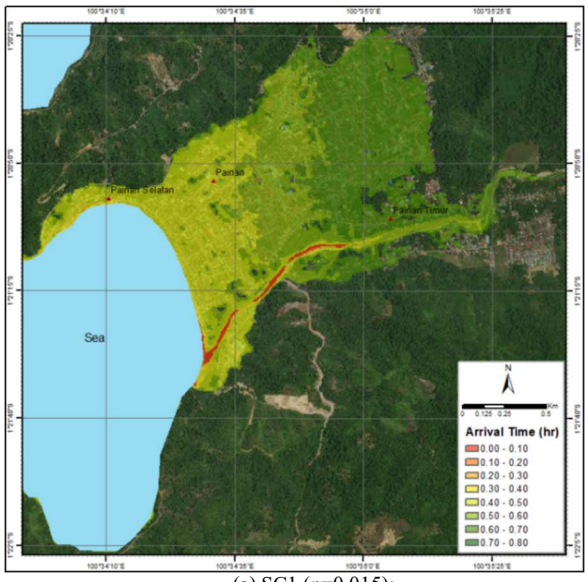

(a) SC1 (n=0.015);

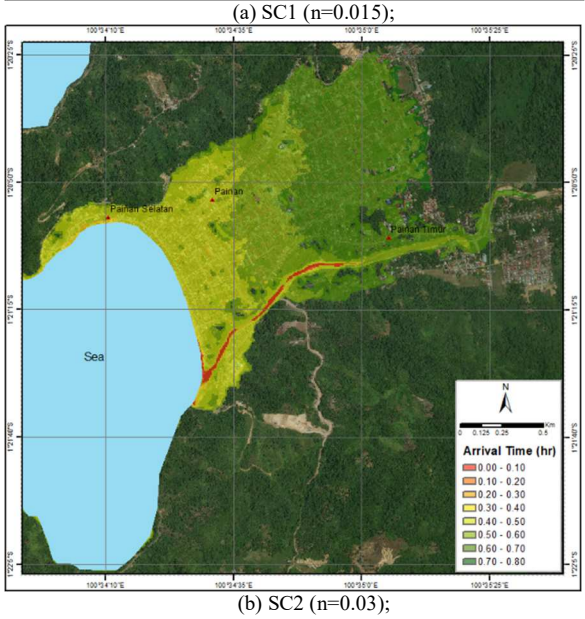

(b) SC2 (n=0.03);

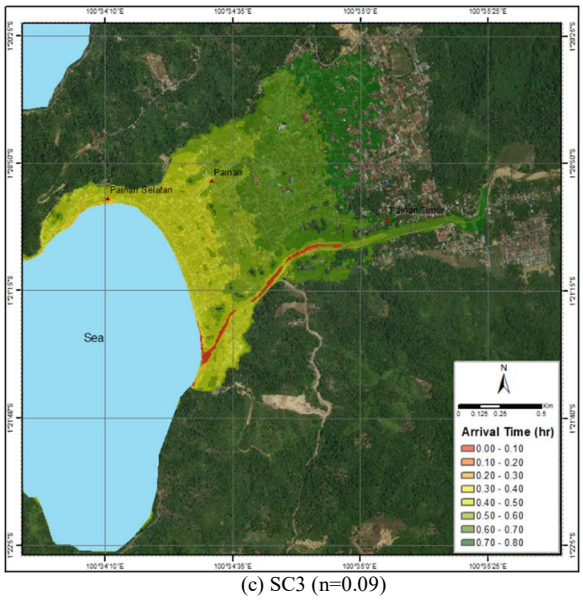

(c) SC3 (n=0.09)

Fig. 13 Arrival time SC1, SC2, and SC3

Here, the surface condition is considered as a high-density urban area with n=0.09. The result shows that the inundation depth near the coast increases significantly. The inundation depth gradually decreased further inland. This indicates a blockage effect due to the surface condition. Hence, the wave cannot penetrate further inland. This shows that placing the mangrove or high structure near the coastline can reduce the tsunami wave.

The simulation results were analyzed further. The velocity distribution for each scenario is shown in Fig. 12. The results show that velocity varies considerably for each scenario. SC1(n=0.015) shows a much higher velocity than that from the other two scenarios (Fig. 12(a)). The velocity of the tsunami overland flow is approximately 6–8 m/s. Smoother surfaces result in higher velocity. The buildings' effect is still quite visible, observed from the topography data from the contoured velocity distribution. SC2 (n=0.03) shows the velocity decreases significantly (Fig. 12(b)). The velocity is approximately 3–5 m/s. Interesting to note that the inundation for both scenarios does not show a significant difference (Fig. 11(a) and 11(b)). This suggests that surface condition affects the flow velocity more than the inundation depth. A significant difference is shown for SC3 (n=0.09). The velocity, in general, is less than 2 m/s. This implies that for a densely populated city, the building in the coastal area acts as a barrier, protecting the inland area and reducing the Tsunami's impact force.

The wave arrival time was assessed for each scenario. The wave arrives at the coastline at the same time for all scenarios (Fig. 13). However, the time travel of the overland flow is different. The wave arrives at the furthest inland in 40 minutes for SC1 (n=0.015), as shown in Fig. 13(a)). The arrival time increases in SC2 (n=0.03). The wave arrives in the northeast area at approximately 44 minutes (Fig. 13(b)). SC3 (n=0.09) showed a much later arrival time, although the inundated area is much closer to the coastline. The wave arrives at the furthest inundation extent at about an hour or more (Fig. 13(c)).

IV. Conclusion

This study simulated the nearshore tsunami in Painan City, West Sumatra, Indonesia. The Tsunami was generated by 8.92 Mw earthquake from the rupture of the Mentawai fault. The tsunami overland flow propagation was simulated using HEC-RAS. The model results show good agreement with those obtained from the previous study using COMCOT. The model can also show the known behavior of tsunami propagation in urban areas and rivers. HEC-RAS demonstrated satisfactory results for practical field simulation with roughness consideration. The simulation can be conducted on other tsunami events and other numerical codes for future works to validate HEC-RAS as an adequate Tsunami overland flow propagation model.

The surface condition plays a significant role in the overland flow. Indonesian topography data already includes building and tree elevation. Therefore, the roughness value for buildings and trees for Indonesia may not follow those proposed by other studies. It was found that the suitable Manning's value for buildings (mid-density urban) and trees is 0.03. Manning's value of 0.015 was applied for road and open areas. Shallow area and river use a manning's value of 0.025.

It was found that the generated Tsunami may reach up to 1875 m inland. The wave arrives on the coast 17 minutes after the rupture. The maximum water depth at the coast is approximately 8.3 m. The averaged inundation depth is approximately 2 - 4 m. The flow velocity is approximately 5 m/s in the city area.

The surface condition's effect on the overland flow was investigated. It was found that there is no significant difference in the inundation depth for open area/road (n=0.015) and mid-density urban/trees (n=0.03). However, the velocity is much lower in the latter case. The high Manning's value acts as a barrier and prevents the wave from propagating further. Hence, it may reduce the impact force of the Tsunami. A high-density urban (n=0.09) surface condition shows a significant reduction in both inundation area and velocity. The high roughness causes blockage. Thus, the Tsunami cannot penetrate further inland. These provide significant information for future mitigation plans. Land cover type is highly important in a nearshore tsunami simulation. Land cover becomes more important when it is found that the historical events of the Tsunami in Indonesia have not affected the consideration of the new location of households in Indonesia.

Consequently, a significant change in land use has taken place in the coastal zone [42]. The situation emerged the importance of land use controls and provided a new mitigation measure. This result is also consistent with the proposed countermeasures whereby in Indonesia, communication, evacuation drills, and land use planning are suggested as the casualty-reduction measures [43]. An accurate representation of the landcover will significantly affect mitigation, e.g., tsunami evacuation buildings and evacuation routes.

Acknowledgment

The authors are grateful for the support given by the Institute for Research and Community Services of Institut Teknologi Bandung through 2020 Multidisciplinary Research entitles "Development of Tsunami Propagation Models for Built Coastal Areas (Pengembangan Model Rambatan Tsunami untuk Kawasan Pantai Terbangun)"

References

[1] U.S. Geological Survey USGS, 2005. (2005) Available: http://earthquake. usgs.gov/eqinthenews/2004/usslav [Accessed: 31 August 2020).

[2] T. Lay, H, Kanamori, C. J. Ammon, M. Nettles, S. N. Ward, R. C. Aster, S. L. Beck, S. L. Bilek, M. R. Brudzinski, R. Butler, H. R. DeShon, G. Ekström, K. Satake, and S. Sipkin. "The great Sumatra-Andaman earthquake of 26 December 2004," Science 308, 1127–1133, 2005.

[3] Syamsidik, M. Al'ala, H. M. Fritz, M. Fahmi, T. M. Hafli. "Numerical simulations of the 2004 Indian Ocean tsunami deposits' thicknesses and emplacements" Nat. Hazards Earth Syst. Sci., 19(6), 1265-1280, 2019.

[4] Q. Qiu, L. Feng, I. Hermawan, P. Banerjee, and D. H. Natawidjaja, "Afterslip following the 2007 Mw 8.4 Bengkulu earthquake in Sumatra loaded the 2010 Mw 7.8 Mentawai tsunami earthquake rupture zone" J. Geophys. Res. Solid Earth, 121, 9034–9049, 2016. doi:10.1002/2016JB013432.

[5] L. Feng, S. Barbot, E. M. Hill, I. Hermawan, P. Banerjee, and D. H. Natawidjaja "Footprints of past earthquakes revealed in the afterslip

of the 2010 Mw 7.8 Mentawai tsunami earthquake", Geophys. Res. Lett., 43, 9518-9526, 2016.
[6] R. Salman, E. M. Hill, L. Feng, E. O. Lindsey, D. Mele Veedu, S. Barbot, P. Banerjee, I. Hermawan, D.H. Natawidjaja "Piecemeal rupture of the Mentawai patch, Sumatra: The 2008 Mw 7.2 North Pagai earthquake sequence" J. Geophys. Res. Solid Earth, 122, 9404–9419, 2017.
[7] D.H. Natawijaya, "Studi Periode Ulang Gempa berdasarkan Pertumbuhan Mikroatol di Mentawai. Simposium Internasional Gempa dan Tsunami," Padang, 2005.
[8] B. Philibosian, K. Sieh, J. Avouac, D.H. Natawidjaja, H. Chiang, C. Wu, C. Shen, M.R. Daryono, H. Perfettini, B.W. Suwargadi, et.al., "Earthquake supercycles on the Mentawai segment of the Sunda megathrust in the seventeenth century and earlier," J. Geophys. Res. Solid Earth, 2012 122, 642–676, 2017.
[9] Pusat Studi Gempa Nasional (PuSGen), "Peta Sumber dan Bahaya Gempa Tahun 2017. 1st ed.; Pusat Penelitian dan Pengembangan Perumahan dan Pemukiman," Badan Penelitian dan Pengembangan: Kementerian Pekerjaan Umum dan Perumahan Rakyat, Indonesia, pp. 182, 189, 2017.
[10] S.C. Singh, N.D. Hananto, A.P.S. Chauhan, H. Permana, M. Denolle, A. Hendriyana, D. Natawidjaja, "Evidence of acrive backthrusting at the NE Margin of Mentawai Islands, SW Sumatra," Geophys. J. Int, 180,703-714, 2010.
[11] J.C. Borrero, "Tsunami inundation modeling for western Sumatra." PNAS, vol. 103 no. 52. 19677, 2006.
[12] J. McCloskey, A. Antonioli, A. Piatanesi, "Tsunami Threat in the Indian Ocean from a Future Megathrust Earthquake West of Sumatra," EPSL, 265(1):61-81, 2008.
[13] A. Muhari, F. Imamura, D.H. Natawidjaja, S. Diposaptono, H. Latief, J. Post, and F.A. Ismail, "Tsunami Mitigation Efforts With pTA In West Sumatra Province, Indonesia," J. of Earthquake and Tsunami, Vol. 04, No. 04, pp. 341-368, 2010.
[14] A. Prasetyo, T. Yasuda, T. Miyashita, N. Mori. "Physical Modeling and Numerical Analysis of Tsunami Inundation in a Coastal City" Front. Built Environ. 5:46, 2019.
[15] V. Titov, F. Gonzalez, "Implementation and Testing of the Method of Splitting Tsunami (MOST) (National Oceanic and Atmospheric Administration, Washington, DC) 1997," Technical Memorandum ERL PMEL-112, Seattle, WA: Pacific Marine Environmental Laboratory, November, 1997, pp. 1–11.
[16] P.S. Rasch, N.H. Pedersen, T. Sato, "Modelling of the Asian Tsunami off the coast of Northern Sumatra", DHI, pp. 1–13, 2017.
[17] L. Li, Z. Huang, Q. Qiu, D.H., Natawidjaja, K. Sieh, "Tsunami-Induced Coastal Change: Scenario Studies for Painan, West Sumatra, Indonesia'" J. of Earth, Planets Sp, Vol. 64, pp. 799-816, 2012.
[18] G.W. Brunner, HEC-RAS, "River Analysis System Hydraulic Reference Manual, version 5.0, U.S. Army Corps of Engineers, Institute for Water Resources," Hydrologic Engineering Center, 2016, pp. 2-53 – 3-60.
[19] M.B. Adityawan, H. Tanaka, "Bed stress assessment under solitary wave run-up," Earth Planet Sp, 64, 12, 2012.
[20] B.P. Yakti, M.B. Adityawan, M. Farid, Y. Suryadi, J. Nugroho, I.K. Hadihardaja, "2D Modeling of Flood Propagation due to Failure of Way Ela Natural Dam," in The Third International Conference on Sustainable Infrastructure and Built Environment (SIBE 2017), Indonesia. Matec Web Conf. 2018, 147 03009.
[21] G.W. Brunner, A. Sanchez, T. Molls, D.A. Parr, "HEC-RAS Verification and Validation Tests, U.S. Army Corps of Engineers, Institute for Water Resources," Hydrologic Engineering Center, 2016, pp. 52 – 55.
[22] J.D. Bricker, S. Gibson, H. Takagi, F. Imamura, "On the need for larger Manning's roughness coefficients in depth-integrated tsunami inundation models", Coastal Engineering Journal 57 (02), 1550005, 2015.
[23] G. Kaiser, L. Scheele, A. Kortenhaus, F. Løvholt, H. R¨omer, S. Leschka, "The influence of land cover roughness on the results of high resolution tsunami inundation modeling," Nat. Hazard and Earth Syst. Sci., 2011.
[24] M. Cramman, R. Coombs, "Fixed and Variable Roughness Regimes for Rapid Inundation Modelling", Smart Dams and Reservoirs, 543-551, 2018.
[25] R. Akoh, T. Ishikawa, T. Kojima, M. Tomaru, S. Maeno, "High-resolution modeling of tsunami run-up flooding: a case study of flooding in Kamaishi city, Japan, induced by the 2011 Tohoku tsunami", Nat. Hazards Earth Syst. Sci., 17, 1871–1883, https://doi.org/10.5194/nhess-17-1871-2017, 2017.
[26] J. D. Jakeman, O. M. Nielsen, K. van Putten, R. Mleczko, D. Burbidge, N. Horspool, "Towards spatially distributed quan-titative assessment of tsunami inundation models," Ocean Dynam, 60(5), 1115–1138, 2010.
[27] M.B. Adityawan, M. Roh, H. Tanaka, A. Mano, K. Udo, "Investigation of tsunami propagation characteristics in river and on land induced by the Great East Japan Earthquake 2011," J. of Earthq. and Tsunami, 2012.
[28] Y.I. Sihombing, M.B. Adityawan, A. Chrysanti, Widyaningtias, M. Farid, J. Nugroho, A.A. Kuntoro, M.A. Kusuma, "Tsunami Overland Flow Characteristic and Its Effect on Palu Bay Due to the Palu Tsunami 2018" J.of Earthq. Tsunami, 14 1-20, 2019.
[29] M.H. Dao, P. Tkalich, "Tsunami propagation modelling – a sensitivity study," Nat. Hazard and Earth Syst. Sci, 2007.
[30] B. Adriano, S. Hayashi, H. Gokon, E. Mas, S. Koshimura, "Understanding the Extreme Tsunami Inundation in Onagawa Town by the 2011 Tohoku Earthquake, Its Effects in Urban Structures and Coastal Facilities", Coastal Engineering Journal, 58:4, 1640013-1-1640013-19, DOI: 10.1142/S0578563416400131, 2016.
[31] H. Yanagisawa, S. Koshimura, T. Miyagi, F. Imamura, "Tsunami damage-reduction performance of a mangrove forest in Banda Aceh, Indonesia inferred from field data and a numerical model", J. Geophys. Res., Vol. 115, C06032, 2010.
[32] D. Tognin, P. Peruzzo, F. De Serio, M. B. Meftah, L. Carniello, A. Defina, M. Mossa, "Experimental Setup and Measuring System to Study Solitary Wave Interaction with Rigid Emergent Vegetation", Sensors, 10.3390/s19081787, 19, 8, (1787), 2019.
[33] G. A. Pasha, N. Tanaka, "Critical Resistance Affecting Sub- to Super-Critical Transition Flow by Vegetation", J.of Earthq. Tsunami, 10.1142/S1793431119500040, (1950004), 2019.
[34] H. Torita, N. Tanaka, K. Masaka, K. Iwasaki, "Effects of forest management on resistance against tsunamis in coastal forests", Ocean Engineering, 10.1016/j.oceaneng.2018.09.013, 169, (379-387), 2018.
[35] K. Forbes and J. Broadhead, "The role of coastal forests in the mitigation of tsunami impacts," Food and Agriculture Organization (FAO) of the United Nations Regional Office for Asia and the Pacific, 2017, http://www.fao.org/forestry/14561-09bf06569b748c827dddf4003076c480c.pdf [accessed November 10, 2019].
[36] S. Koshimura, S. Hayashi, "Tsunami flow measurement using the video recorded during the 2011 Tohoku tsunami attack." In 2012 IEEE International Geoscience and Remote Sensing Symposium, Munich, Germany, 2009, pp. 6693 – 6696.
[37] M. Kotani, F. Imamura, N. Shuto, "Tsunami run-up simulation and damage estimation by using geographical information system," Proc. Coastal Eng, 45, 356-360 (in Japanese), 1998.
[38] E. M. Hill, J.C. Borrero, Z. Huang, Q. Qiu, P. Banerjee, D.H. Natawidjaja, P. Elosegui, H.M. Fritz, B.W. Suwargadi, I.R. Pranantyo, et.al., "The 2010 Mw 7.8 Mentawai earthquake: Very shallow source of a rare tsunami earthquake determined from tsunami field survey and near-field GPS data," J. Geophys. Res., 117, B06402, 2012.
[39] Google earth V 7.3.3.7699. (February 13, 2019). Painan, West Sumatra. 47 S 676,829.18 m E and 984,9202.47 m S, Eye alt 5.56 km. CNES/Airbus, Maxar Technologies, AfriGIS (Pty) Ltd. http://www.earth.google.com [Accessed: 27 July 2020].
[40] H. Tanaka, K. Kayane, M. B. Adityawan, M. Roh, M. Farid, "Study on the relation of river morphology and tsunami propagation in rivers," Ocean Dyn, 64(9), 1319–1332, 2014.
[41] Y. Aoyama, M.B. Adityawan, W. Widiyanto, Y. Mitobe, D. Komori, H. Tanaka, "Numerical Study on Tsunami Propagation into a River," J. of Coast. Res, 75 (sp1), 1017-1021, 2016.
[42] Syamsidik, R.S. Oktari, K. Munadi, S. Arief, I. Z. Fajri, "Changes in coastal land use and the reasons for selecting places to live in Banda Aceh 10 years after the 2004 Indian Ocean tsunami", Nat Hazards 88, 1503–1521, https://doi.org/10.1007/s11069-017-2930-3, 2017.
[43] T. Otake, C. T. Chua, A. Suppasri, F. Imamura, "Justification of Possible Casualty-Reduction Countermeasures Based on Global Tsunami Hazard Assessment for Tsunami-Prone Regions over the Past 400 Years," J. Disaster Res., Vol.15, No.4, pp. 490-502, 2020.